Single-Electron Transport through Single Dopants in a Dopant-Rich Environment

Michiharu Tabe,[1,*] Daniel Moraru,[1] Maciej Ligowski,[1,2] Miftahul Anwar,[1] Ryszard Jablonski,[2] Yukinori Ono,[3] and Takeshi Mizuno[1]

[1]*Research Institute of Electronics, Shizuoka University, 3-5-1 Johoku, Naka-ku, Hamamatsu 432-8011, Japan*
[2]*Division of Sensors and Measuring Systems, Warsaw University of Technology, A. Boboli 8, Warsaw 02-525, Poland*
[3]*NTT Basic Research Laboratories, NTT Corporation, 3-1 Morinosato Wakamiya, Atsugi, Kanagawa 010-8502, Japan*
(Received 25 September 2009; published 2 July 2010)

We show that single-electron transport through a single dopant can be achieved even in a random background of many dopants without any precise placement of individual dopants. First, we observe potential maps of a phosphorus-doped channel by low-temperature Kelvin probe force microscopy, and demonstrate potential changes due to single-electron trapping in single dopants. We then show that only one or a small number of dopants dominate the initial stage of source-drain current vs gate voltage characteristics in scaled-down, doped-channel, field-effect transistors.

DOI: 10.1103/PhysRevLett.105.016803 PACS numbers: 73.23.Hk, 73.20.Hb, 73.61.Cw, 73.63.Bd

Semiconductor devices using a single dopant atom are attractive because they may open a new paradigm in nanodevice physics. Single-electron transport through one or a few dopant atoms in low-doped channels of field-effect transistors (FETs) has recently been characterized experimentally [1–4] and theoretically [5–7]. An ionized dopant atom can work as a quantum dot (QD), and electrons tunnel one by one through the dopant coupled to electrodes. This "atom" structure has been considered the building block for applications such as quantum computing [8,9], single-electron transfer [10–12], and single-dopant ionization detection [13]. Recent progress in dopant engineering [14–16] and dopant mapping techniques [17,18] is promising for improving the understanding of single-dopant devices. However, controlling the position and the number of individual dopants remains a huge challenge. Nanostructures containing many dopant atoms can be, on the other hand, fabricated with conventional doping techniques. It is essential to understand if electron transport is controlled by individual dopants even in such many-dopant environments. The overall potential landscape is modulated by the superposed potentials of many dopants [19–22]. For nanostructures doped with phosphorus (P), the lowest electronic potential will be formed close to the channel center due to the entire set of dopants. When the channel minimum conduction band energy is shifted close to the source Fermi level by gate voltage, transport occurs through the dopant-induced QDs. In this Letter, we first report direct observations of potential changes due to single-electron trapping in dopant potentials. Then, we show by electrical measurements and simulation that in scaled-down doped-channel FETs, the structure of the dopant-induced QD arrays can be statistically controlled.

First, we monitored the electronic potential profiles at the surface of a P-doped-nanoscale Si channel. For that, we used low-temperature Kelvin probe force microscopy (KFM). In the KFM technique [23], a conducting cantilever is scanned over the sample surface at a constant height. At each measurement point, the electrostatic force that builds up between the cantilever and the sample is nullified by a dc voltage that corresponds to the actual time-averaged surface electronic potential. KFM can thus sense electrostatic force through a thermally grown SiO_2 layer due to charges within a few nanometers below the interface. Such depth sensitivity of the KFM is a strong advantage over other dopant mapping techniques, since one can monitor changes in potential profiles almost simultaneously while the device is working. In our previous work [18], we have already shown that, in conventionally doped silicon FETs ($N_d \approx 1 \times 10^{18}$ cm^{-3}), features ascribable to individual ionized dopants can be identified.

The devices for KFM observation were fabricated on silicon-on-insulator (SOI) substrates and have a channel defined by an electron beam lithography technique as a constriction of 200 nm length and 150 nm width connected to wider pads of Si for source and drain. The top Si was uniformly doped with phosphorus diffused from a spin-coated silica film containing phosphorus oxide (P_2O_3). Doping concentration was estimated to be $N_d \approx$ 1–3×10^{18} cm^{-3}, which corresponds to an interdopant distance of 7–10 nm. We estimated this value from secondary ion mass spectrometry depth profiles of control samples fabricated by the same doping treatments as the device samples. The randomly distributed dopants are expected to create a nonuniform potential within the device channel. A thin SiO_2 layer ($\sim$2 nm) was thermally grown by dry oxidation at 900 °C for 1 min in purified oxygen gas in an industry-grade quartz tube furnace located in a cleanroom. This provides a Si/SiO_2 interface basically free of gap states within the KFM scanning area. The final channel thickness was 20 nm. The measurement setup and schematic device structure are shown in Fig. 1(a).

In order to observe the dopant-induced potential landscape, it is necessary to deplete the channel of free carriers that could screen the dopant potentials [18]. Semiconductor quantum dots induced by dopant atoms have been

 © 2010 The American Physical Society

previously characterized by scanning tunneling microscopy at room temperature [24–26]. It was shown that the ability to deplete the dots by the tip's electric field is reduced compared to spatially unconfined material. In our work, we perform the measurements at low temperature (13.7 K); therefore, most dopants are neutralized without thermal emission of electrons under low electric fields. However, the substrate Si and two side gates were biased at $V_g = -4$ V, which is large enough to deplete the donor electrons and to observe the bare donor ions without screening by the carrier electrons. The KFM scanning area is 120×120 nm^2 centered on the constriction channel, thus practically covering 80% of the channel width.

Figure 1(b) shows the electronic potential map measured at source-drain bias $V_{sd} = 0$ mV. The contrast is defined so that higher electronic potential (larger negatively charged) areas correspond to brighter contrast. The nonuniform potential is due to the presence of ionized P impurities [20,21,27]. We counted 90–120 fine potential fluctuations (dark spots) with radii of 2–4 nm and depths of 10–30 mV in the measured KFM images. This value is in good agreement with the estimated number of dopants located within about 5 nm from the surface in the scanning area. The spatial extension of the dark spots is comparable to the Bohr radius for P in Si of 2.3–3 nm [1,5,7,27,28], suggesting that they usually originate from single dopant atoms. The potential depth is less than 46 meV, which is the first binding energy of a P dopant in bulk Si [28]. However,

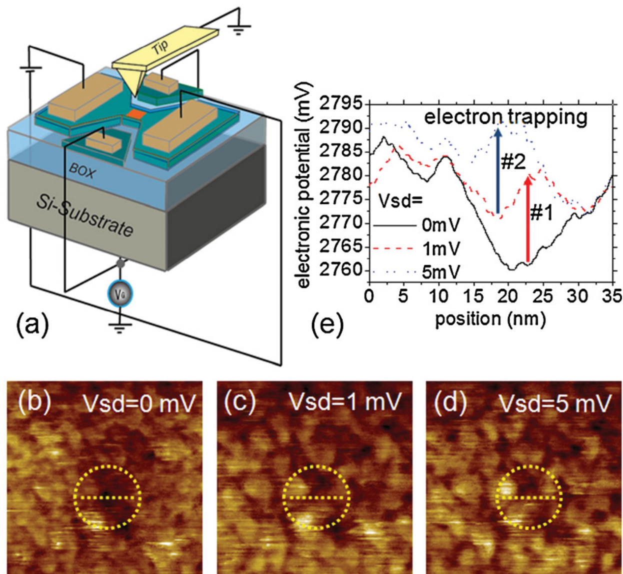

FIG. 1 (color). (a) SOI-FET structure [the substrate Si is used as a back gate coupled to the channel through a 400 nm-thick buried oxide (BOX) layer] and schematic KFM measurement setup (the measurement area is indicated on the channel). (b), (c), (d) Surface potential maps (120×120 nm^2) of doped-nanoscale FETs for $V_{sd} = 0$, 1, and 5 mV, respectively. The region where charging effects are most prominent is marked. (e) Line profiles [as marked in (b), (c), and (d)] indicating a local increase of potential with increasing V_{sd}.

since the KFM monitors the potential at the surface of the channel, the observed values of 10–30 mV may correspond to ionized dopants located a few nanometers below the surface. In the low-temperature regime of our measurements, each P dopant accommodates one electron. For the results shown in Fig. 1(b), the channel is depleted of free carriers by a negatively large gate voltage ($V_g = -4$ V); also, the source-drain bias is zero ($V_{sd} = 0$ mV). In this system, we then apply small source-drain biases {$V_{sd} = 1$ mV [Fig. 1(c)] and $V_{sd} = 5$ mV [Fig. 1(d)]}, corresponding to the continuous flow of electrons at source-drain currents $I_{sd} \approx 1$ nA and $I_{sd} \approx 10$ nA, respectively. The potential maps change as a result of electron trapping and electron flowing through dopants. From these measurements, we cannot clearly identify the actual conduction path. However, in order to distinguish single-electron trapping events, we focus on the encircled region that contains the lowest potential observed in the channel at $V_{sd} = 0$ mV. It is most likely that electrons will occupy this low-potential region. Line profiles taken in this area are shown in Fig. 1(e). In order to remove the effect of background potential changes, we added 5 mV and 10 mV to the line profiles for $V_{sd} = 1$ mV and $V_{sd} = 5$ mV, respectively. The displacement is possibly due to the long-range effect of charging in the vicinity of the region of interest. In this way, the line profiles were aligned and we observed that the potential minimum increased by 22 mV for $V_{sd} = 1$ mV and by 21 mV for $V_{sd} = 5$ mV. Considering the localization of these potential increments and their values, we ascribe each of these observations to single-electron trapping events (event #1 and event #2 in Fig. 1(e)] in two different neighboring dopants located about 5 nm from each other. These results suggest that even in many-dopant systems, single-electron–single-dopant interactions can be distinguished.

For understanding single-electron transport properties of P-doped nanostructures, we measured the source-drain current (I_{sd}) vs gate voltage (V_g) characteristics for highly scaled-down FETs. The devices were fabricated similarly to the ones used for KFM observation, but channel constrictions of smaller lengths (20–150 nm) were defined between the two wider fan-shaped pads of Si for the source and drain [channel structure is shown in Figs. 2(a) and 2(d)]. After gate oxidation for a 10 nm-thick SiO_2, a wide Al front gate was formed. Doping concentration was estimated to be $N_d \approx 1$–5×10^{18} cm^{-3}. This means that in the device channel there are many dopants that modulate its potential. Figure 2 (middle panels) shows typical examples of dopant-induced potential landscapes simulated for random arrangements of dopant atoms with Coulombic potentials (doping concentration $N_d = 1 \times 10^{18}$ cm^{-3}) in a short nanostructure [Fig. 2(b)] and a long nanostructure [Fig. 2(e)]. It can be observed that the center of the channel has a lower potential due to the cumulative effect of the surrounding dopants. Conduction starts when the channel minimum potential is shifted close to the source Fermi level by applying a positive V_g to the gate. It is expected

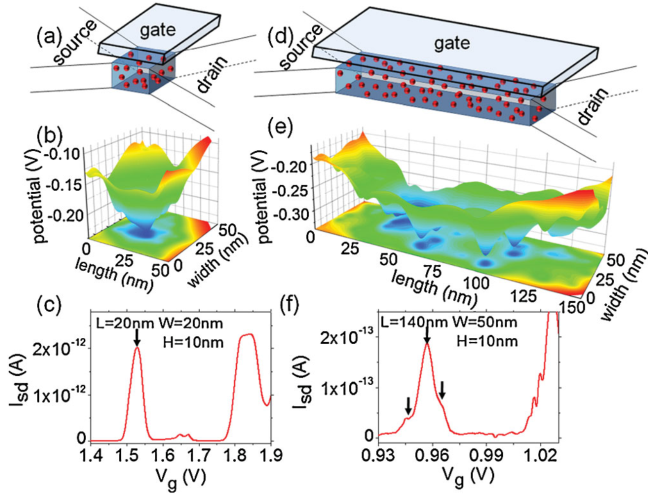

FIG. 2 (color). (a) Schematic channel structure, (b) example of simulated potential profile, (c) example of dc $I_{\rm sd} - V_g$ characteristics ($V_{\rm sd} = 5$ mV) for a short-channel FET. (d) Schematic channel structure, (e) example of simulated potential profile, (f) example of dc $I_{\rm sd} - V_g$ characteristics ($V_{\rm sd} = 5$ mV) for a long-channel FET. The arrows in 2(c) and 2(f) indicate the location of the inflections (i.e., subpeaks).

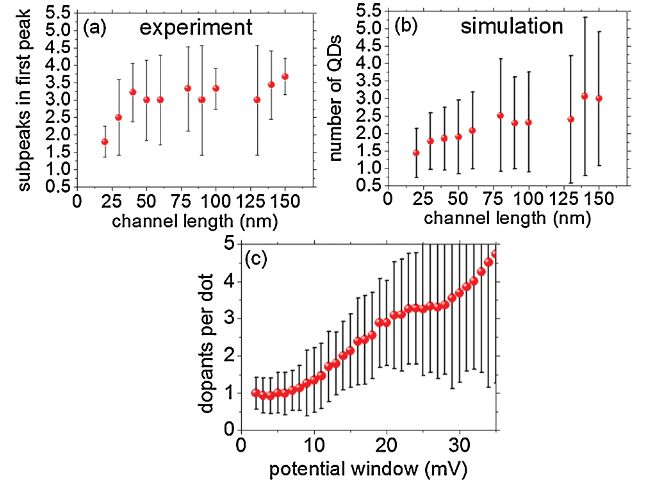

FIG. 3 (color). (a) Statistical results of the number of subpeaks incorporated in the first peak of the $I_{\rm sd} - V_g$ characteristics as a function of channel length (5–10 devices were measured for each case). (b) Statistical results of the number of dopant-induced QDs as a function of channel length obtained from simulations of 50 different dopant arrangements for each case. (c) Average number of dopants embedded in one QD for 50×50 nm^2 nanostructures as a function of a potential window measured from the bottom of the well formed in the channel.

that one dopant or an array of a few dopants with comparable potentials will control the initial stages of transport. The $I_{\rm sd} - V_g$ characteristics contain nonperiodic current oscillations, which can be ascribed to single-electron tunneling through dopant-induced QDs. The two lower panels in Fig. 2 show the first peaks (first observable current peaks above 10 fA, when V_g is increased) of $I_{\rm sd} - V_g$ characteristics measured at 17 K for FETs with constriction lengths of 20 nm [Fig. 2(c)] and 140 nm [Fig. 2(f)]. As a statistical tendency, short-channel FETs exhibit smooth single-peak (or double-split peak) current oscillations, while longer-channel FETs typically exhibit multiple-split peak features (or inflections). The observed inflections are marked by arrows in Figs. 2(c) and 2(f). The splitting of a current peak is an indication of the formation of a multiple-QD array in the channel, while the number of subpeaks can be considered an indication of the number of QDs [29]. Therefore, our results suggest a dependence of the number of QDs on the channel length.

To provide a statistical image of our results, we counted the number of subpeaks in the first measured current peak for 5–10 devices for each channel length ($L_{\rm ch}$) value ($L_{\rm ch}$ was changed in 11 steps from 20 to 150 nm). Figure 3(a) contains the statistical results of the average number of subpeaks (dot symbols) and the standard deviation from the average (error bars). Although the dispersion of the data is considerable, it is obvious that there is an increasing trend in the number of subpeaks (i.e., the number of dopant-induced QDs) with $L_{\rm ch}$.

In order to clarify this point, we performed statistical simulations and, for simplicity, we studied the behavior of isolated channels in the absence of the influence from source or drain doping. We considered nanostructures of different lengths (20–150 nm), but of the same width (50 nm) and thickness (10 nm). In these structures, we randomly introduced dopants with Coulombic potentials [18,30] to a concentration $N_d = 1 \times 10^{18}$ cm^{-3}. The potential at each point is the result of the superposition of all dopant potentials. For monitoring the QD array structure, we chose a potential window of 30 mV from the bottom of the channel potential. This value is close to our approximate estimation of the charging energy from the experimental characteristics. We define as the QD a three-dimensional region containing points within the chosen potential window and completely surrounded by points of higher potential (i.e., barriers). Figure 3(b) plots the average number of QDs (dot symbols) obtained from 50 different dopant arrangements for each $L_{\rm ch}$ case. The number of QDs exhibits, indeed, an increasing trend as a function of $L_{\rm ch}$. The trend is in good agreement with the experimental results, indicating that the number of dopant QDs is statistically controllable by the channel length.

It is also essential to evaluate the number of dopant atoms incorporated in each QD. Figure 3(c) shows the number of dopants per QD statistically estimated from simulation for 50×50 nm^2 nanostructures ($N_d = 1 \times 10^{18}$ cm^{-3}). In this simulation, we used a potential window with the lower level fixed at the bottom of the potential in the channel. We gradually increased the higher level of the potential window and monitored the number of dopants and the number of QDs inside the window. It can be observed that within a window of about 10 mV, each QD contains, on average, one dopant. At around 30 mV, the

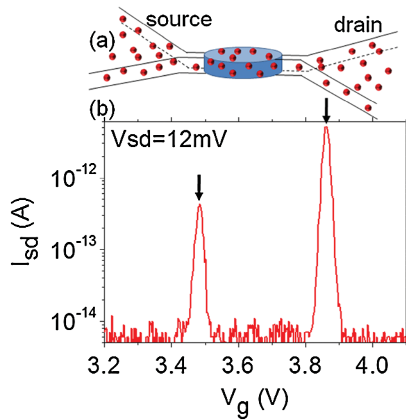

FIG. 4 (color). (a) Schematic channel structure of the isolated disk-shaped-channel FET and (b) the dc $I_{sd} - V_g$ characteristics. Arrows indicate two smooth peaks.

average number of dopants in each QD is about 3. Since single-electron tunneling occurs soon after the lowest channel potential is aligned with the source or drain Fermi level, it is reasonable to assume that, within this small window, each QD contains only one dopant atom.

It is expected that transport through single-dopant QDs can be achieved with higher probability in patterned channels, significantly isolated from source and drain extensions [31]. We investigated devices having disk-shaped channels (with a radius of about 50 nm) connected to the source and drain by narrow constrictions. The channels are doped similarly to the previous devices ($N_d \approx 1–5 \times 10^{18}$ cm^{-3}). The schematic channel structure is shown in Fig. 4(a). Because of the radial symmetry of the channels, the potential in the center of the disk will be lower than at its edges as a result of the superposed effect of many dopants, and thus it is more likely that a single QD will be formed in the channel. The $I_{sd} - V_g$ characteristics measured at 17 K are shown in Fig. 4(b). The characteristics indeed exhibit single-peak features for the first observable current peaks, which is a signature of the creation of a single QD in the channel. The difference between the peak positions in V_g is large (~400 mV). In the model of a single metallic QD, this gives a gate capacitance of 0.4 aF, which is inconsistent with calculations based on the geometry of our devices. Therefore, the two observed peaks arise due to single-electron transport through different single-dopant QDs. This result presents the capability of controlling transport through single dopants by combining nanopatterns and the effect of the superposition of many dopants. Further optimization can be achieved through studies on the correlation between channel patterns, dopant concentration, and device characteristics.

In conclusion, we demonstrated that single-electron transport through single-dopant dots can be achieved even in random dopant-rich environments. This is due to the effect of the large number of dopant atoms that create a potential landscape favorable for accessing even a single dopant atom. The findings presented here open a door for designing single-dopant transistors using conventional doping technology, with applications to a variety of future devices such as quantum computers.

This work was partially supported by KAKENHI (No. 16106006, No. 18063010, and No. 20241036). We thank Y. Kasai, K. Ebisawa, S. Miki, and R. Nakamura for their support during experiments.

*romtabe@rie.shizuoka.ac.jp

[1] H. Sellier *et al.*, Phys. Rev. Lett. **97**, 206805 (2006).
[2] Y. Ono *et al.*, Appl. Phys. Lett. **90**, 102106 (2007).
[3] G. P. Lansbergen *et al.*, Nature Phys. **4**, 656 (2008).
[4] M. A. H. Khalafalla *et al.*, Appl. Phys. Lett. **91**, 263513 (2007).
[5] A. S. Martins, R. B. Capaz, and B. Koiller, Phys. Rev. B **69**, 085320 (2004).
[6] C. J. Wellard and L. C. L. Hollenberg, Phys. Rev. B **72**, 085202 (2005).
[7] M. J. Calderon *et al.*, Phys. Rev. Lett. **96**, 096802 (2006).
[8] B. E. Kane, Nature (London) **393**, 133 (1998).
[9] L. C. L. Hollenberg *et al.*, Phys. Rev. B **69**, 113301 (2004).
[10] D. Moraru *et al.*, Phys. Rev. B **76**, 075332 (2007).
[11] D. Moraru *et al.*, Appl. Phys. Express **2**, 071201 (2009).
[12] K. Yokoi *et al.*, Jpn. J. Appl. Phys. **48**, 024503 (2009).
[13] Z. A. Burhanudin, R. Nuryadi, and M. Tabe, Appl. Phys. Lett. **91**, 042103 (2007).
[14] S. R. Schofield *et al.*, Phys. Rev. Lett. **91**, 136104 (2003).
[15] T. Shinada *et al.*, Nature (London) **437**, 1128 (2005).
[16] F. J. Rueß *et al.*, Small **3**, 563 (2007).
[17] M. Nishizawa, L. Bolotov, and T. Kanayama, Appl. Phys. Lett. **90**, 122118 (2007).
[18] M. Ligowski *et al.*, Appl. Phys. Lett. **93**, 142101 (2008).
[19] J. H. Davies and J. A. Nixon, Phys. Rev. B **39**, 3423 (1989).
[20] R. A. Smith and H. Ahmed, J. Appl. Phys. **81**, 2699 (1997).
[21] T. Koester *et al.*, Jpn. J. Appl. Phys. **38**, 465 (1999).
[22] A. Tilke *et al.*, J. Appl. Phys. **89**, 8159 (2001).
[23] M. Nonnenmacher, M. P. O'Boyle, and H. K. Wickramasinghe, Appl. Phys. Lett. **58**, 2921 (1991).
[24] N. D. Jäger *et al.*, Appl. Phys. Lett. **82**, 2700 (2003).
[25] S. Landrock *et al.*, Appl. Phys. Lett. **95**, 072107 (2009).
[26] A. Laubsch, K. Urban, and Ph. Ebert, Phys. Rev. B **80**, 245314 (2009).
[27] A. K. Ramdas and S. Rodriguez, Rep. Prog. Phys. **44**, 1297 (1981).
[28] L. M. Kettle *et al.*, Phys. Rev. B **68**, 075317 (2003).
[29] F. R. Waugh *et al.*, Phys. Rev. Lett. **75**, 705 (1995).
[30] G. J. Evans, H. Mizuta, and H. Ahmed, Jpn. J. Appl. Phys. **40**, 5837 (2001).
[31] Y. Takahashi *et al.*, Electron. Lett. **31**, 136 (1995).